Protoplasma (2013) 250:495–503
DOI 10.1007/s00709-012-0432-4

ORIGINAL ARTICLE

Development of flange and reticulate wall ingrowths in maize (*Zea mays* L.) endosperm transfer cells

Paulo Monjardino · Sara Rocha · Ana C. Tavares · Rui Fernandes · Paula Sampaio · Roberto Salema · Artur da Câmara Machado

Received: 1 June 2011 / Accepted: 5 July 2012 / Published online: 20 July 2012

Abstract Maize (*Zea mays* L.) endosperm transfer cells are essential for kernel growth and development so they have a significant impact on grain yield. Although structural and ultrastructural studies have been published, little is known about the development of these cells, and prior to this study, there was a general consensus that they contain only flange ingrowths. We characterized the development of maize endosperm transfer cells by bright field microscopy, transmission electron microscopy, and confocal laser scanning microscopy. The most basal endosperm transfer cells (MBETC) have flange and reticulate ingrowths, whereas inner transfer cells only have flange ingrowths. Reticulate and flange ingrowths are mostly formed in different locations of the MBETC as early as 5 days after pollination, and they are distinguishable from each other at all stages of development. Ingrowth structure and ultrastructure and cellulose microfibril compaction and orientation patterns are discussed during transfer cell development. This study provides important insights into how both types of ingrowths are formed in maize endosperm transfer cells.

Handling Editor: David McCurdy

P. Monjardino (✉) · S. Rocha · A. C. Tavares · A. da Câmara Machado
Instituto de Biotecnologia e Bioengenharia—Centro de Biotecnologia dos Açores, Universidade dos Açores, 9701-851 Angra do Heroísmo, Portugal
e-mail: paulo@uac.pt

R. Fernandes · P. Sampaio · R. Salema
IBMC-Instituto de Biologia Molecular e Celular, Universidade do Porto, Rua do Campo Alegre, 4150-180 Porto, Portugal

R. Salema
Departamento de Biologia, Faculdade de Ciências, Universidade do Porto, Rua do Campo Alegre, 4150-180 Porto, Portugal

Keywords Transfer cells · Maize endosperm · Reticulate ingrowths · Flange ingrowths

Abbreviations

MBETC	Most basal endosperm transfer cells
CLSM	Confocal laser scanning microscopy
DAP	Days after pollination
GDD	Growing degree days
OPW	Outer periclinal wall
TEM	Transmission electron microscopy

Introduction

Maize endosperm is a triploid storage tissue accounting for up to 80 % of the kernel biomass. There are three major cell types in the endosperm: the cells that accumulate starch and protein (starchy endosperm), the aleurone layer, and the transfer cells (Becraft 2001; Becraft and Yi 2011). The starchy endosperm is further divided into specialized regions known as the sub-aleurone, the embryo-surrounding region, and the conducting zone (Becraft 2001).

The transfer cells are located in the placento-chalazal region adjacent to the main vascular tissues of the pedicel, they extend up to six cells in depth (Davis et al. 1990) and are the first cells to differentiate in the endosperm, commencing approximately 6 days after pollination (DAP) (Charlton et al. 1995; Becraft 2001). These cells have adapted to transport assimilates into the starchy endosperm cells and they undergo a characteristic form of cell wall growth in which uneven thickenings ultimately develop into distinct ingrowths. Potentially, the transport capacity is enhanced by amplification of plasmalemma surface area and by enrichment of transporters, thus facilitating the apo/symplasmic transport of solutes (Offler et al. 2003). After several weeks, the transfer cells undergo senescence during the stage at

which most of the endosperm is at an advanced stage of apoptosis (Young and Gallie 2000).

Reticulate or flange ingrowths form in transfer cells of many species (Gunning and Pate 1969; Talbot et al. 2002; Offler et al. 2003; McCurdy et al. 2008), although in only a few studies has it been recognized that they coexist in the same cells (Talbot et al. 2002; Pugh et al. 2010). Reticulate wall ingrowths are more common and have a unique morphology, emerging as small projections or papillae from the underlying wall at discrete but apparently random loci, then branching and often fusing laterally to form a fenestrated layer of wall material that will ultimately become a multi-layered labyrinth (Talbot et al. 2001, 2007b; Offler et al. 2003; McCurdy et al. 2008). Cellulose deposition is the driving force in the prevailing model for reticulate wall ingrowth formation following the emergence of discrete papillae (Talbot et al. 2007b; McCurdy et al. 2008). Tangled and apparently disorganized microfibrils form near the plasma membrane with no relationship to the microfibrils of the underlying primary cell wall, and the papillae emerge from raised patches that accumulate more material than surrounding areas (Talbot et al. 2001, 2007b), probably reflecting that cellulose synthase complexes are delivered to the plasma membrane randomly and directed by microtubules (McCurdy et al. 2008).

Flange wall ingrowths form thin ribs as well as broad flat or thick and anastomosed sheet structures (Talbot et al. 2002, 2007a) superficially resembling the secondary wall thickenings of tracheary elements, although they may not be lignified (Gunning and Pate 1974; Vaughn et al. 2007). The wall material appears to be deposited progressively along the full length of these structures, eventually producing a complex, dense network of ingrowth material characterizing the elaborate and often branched/interwoven flange morphology (Talbot et al. 2002; McCurdy et al. 2008). Flange wall ingrowths involve the organization of cellulose microfibrils that are more densely packed than reticulate ingrowths as revealed by transmission electron microscopy (TEM) (Davis et al. 1990; Talbot et al. 2002; Offler et al. 2003). Flange ingrowth projections arise from the addition of more microfibrils, the cellulose must be deposited by cellulose synthase complexes following microtubules (Offler et al. 2003; Talbot et al. 2007a; McCurdy et al. 2008).

Wall ingrowths have a very similar composition as compared with the adjacent primary walls. Studies showed that cellulose, xyloglucan, and pectins are distributed uniformly within the wall (Vaughn et al. 2007), but extensins, arabinogalactan proteins, and callose are distributed with distinct patterns in reticulate ingrowths (Dahiya and Brewin 2000; Vaughn et al. 2007). The chemical composition of transfer cell wall ingrowths is essentially the same as that of archetypical cell walls, suggesting any morphological differences do not reflect underlying differences in composition (DeWitt et al. 1999; Vaughn et al. 2007).

Maize endosperm transfer cells are considered to contain flange ingrowths that are thin and rib shaped, becoming progressively crossed-linked and fused towards the base of the cell (Davis et al. 1990; Felker and Shannon 1980; Talbot et al. 2002, 2007a; Offler et al. 2003; McCurdy et al. 2008; Kang et al. 2009). Next to the outer periclinal wall (i.e., the peripheral periclinal wall of the most basal endosperm transfer cells (MBETC) adjacent to the placental cavity—outer periclinal wall (OPW)), lateral protrusions that resemble those in reticulate wall ingrowths, appear to be spatially coordinated and will create an extensive branching of the flange ingrowths (Talbot et al. 2002; McCurdy et al. 2008). In the MBETC, the wall material fills most of the cell lumen, comprising anastomosed ribs in the apical portion and a dense network of wall material in the basal portion (Talbot et al. 2002, 2007a), but in the inner transfer cells, there is a gradual reduction on the numbers and extension of ingrowths the further they are away from the OPW (Davis et al. 1990). Our developmental analysis of maize endosperm transfer cell differentiation showed that the MBETC develop flange and reticulate wall ingrowths simultaneously but in separate regions, whereas the inner transfer cells only form flange ingrowths. The formation patterns of both ingrowths are discussed.

Materials and methods

Plant material, growth conditions, and sampling

Maize seeds (*Zea mays* L., inbred W64A) were planted in a naturally lit greenhouse in 20-L pots containing Andosol loam soil (in 2009 and 2011) at the Universidade dos Açores campus of Angra do Heroísmo. Plants were fertilized weekly, alternating 3 g of commercial fertilizer (20/5/10) with 100 mL of Hoagland's solution per pot (Hoagland and Arnon 1938). Controlled pollinations were carried out on all test plants.

The temperature was recorded daily during early kernel development allowing the calculation of growing degree days (GDD) according to the formula $GDD=\Sigma(ADT-BT)$, where ADT is the average daily temperature and BT is the base temperature of 10 °C (Gilmore and Rogers 1958). Minimum temperatures <10 °C were adjusted to 10 °C, and maximum temperatures >30 °C were adjusted to 30 °C. The developmental stages were therefore described as DAP and references were made to GDD.

For each sampling date, 35 to 50 kernels were collected from at least 9 different ears, and endosperm transfer cells located between the germinal side and the mid placento-chalazal region were analyzed.

Bright field microscopy

Tissues were prepared and fixed in two alternative ways: (1) kernels were sectioned longitudinally (200–500 μm thickness) with a Leica VT 1200 vibratome (Leica Microsystems,

Wetzlar, Germany) in 4 % paraformaldehyde plus 0.1 % glutaraldehyde in a buffer containing 60 mM PIPES, 25 mM HEPES, 2 mM $MgCl_2$, 10 mM EGTA and 5 % dimethylsulfoxide at pH 6.9 (PHEM/DMSO), and after sectioning were fixed in 4 % glutaraldehyde plus 4 % paraformaldehyde in PIPES buffer and second postfixed in 2 % osmium tetroxide in the same buffer (Salema and Brandão 1973) for 2 h at room temperature in each step (Monjardino et al. 2007); (2) kernels were hand sectioned with a razor blade, discarding most of the endosperm tissue except for the basal endosperm region, and were immediately fixed in 4 % glutaraldehyde plus 2 % osmium tetroxide for 2 h. The fixed sections were dehydrated in acetone and progressively infiltrated in Spurr's resin over 8 days at room temperature (Monjardino et al. 2007) before polymerization at 60 °C. Most of the images were obtained from samples that were prepared with the first methodology.

Semi thin sections (400–800 nm thickness) were obtained on a LKB 2188 NOVA Ultramicrotome (LKB NOVA, Bromma, Sweden) using glass knives. The sections were transferred to glass slides, stained with toluidine blue, examined under a Zeiss microscope Axioimager A1 (Carl Zeiss Oberkochen, Germany) and images were recorded with a Zeiss digital camera Axiocam MRc.

Transmission electron microscopy

Samples were obtained as in bright field microscopy, but most of the images were obtained from samples that were prepared and fixed with the second methodology. Ultrathin sections (40–60 nm thickness) were prepared on a LKB 2188 NOVA Ultramicrotome (LKB NOVA, Bromma, Sweden) using diamond knives (DDK, Wilmington, DE, USA). The sections were mounted on 200 mesh copper or nickel grids, stained with uranyl acetate and lead citrate for 15 min each, and examined under a JEOL JEM 1400 TEM (Tokyo, Japan). Images were digitally recorded using a Gatan SC 1000 ORIUS CCD camera (Warrendale, PA, USA).

Confocal laser scanning microscopy

Kernels were sectioned longitudinally (70–100 μm thicknesses) on a Leica VT 1200 vibratome in 4 % paraformaldehyde plus 0.1 % glutaraldehyde in PHEM/DMSO buffer for 2 h, after which the sections were washed in a buffer containing 137 mM NaCl, 2.7 mM KCl, 40.2 mM Na_2HPO_4, and 17.6 mM KH_2PO_4 at pH 7.4 (PBS), stained with filtered 0.01 % calcofluor white for 1 min, and washed again in PBS buffer. Sections were visualized under a Zeiss confocal laser scanning microscopy (CLSM) 510 with excitation λ at 405 nm (UV diode laser) and detection at 420–480 nm. The projected images were obtained from Z stacks at a resolution of 1,024× 1,024 pixels. The Z stacks contained 22–60 planes at 0.37 μm intervals. All selected images were imported into Adobe Photoshop CS software (Adobe Systems, San Jose, CA) for presentation and photomontages were produced in the same software.

Results

Flange and reticulate ingrowth development occurred mostly from 5 to 12 DAP (75–192 GDD), although there were still some variations in their ultrastructure up to 20 DAP (302–318 GDD, Figs. 1, 2, and 3). The MBETC developed both flange and reticulate ingrowths, whereas the inner transfer cells only developed flange ingrowths (Figs. 2 and 3). The higher density of ingrowths in the MBETC must have been responsible for staining more intensively, especially after 10 DAP (Fig. 1b–d). Ingrowth composition, regardless of being reticulate or flange, probably is not the cause of such differences (Offler et al. 2003) because it usually is similar to the adjacent primary wall (DeWitt et al. 1999; Dahiya and Brewin 2000; Vaughn et al. 2007).

The further away the transfer cells were from the OPW, the shorter the flange ingrowths (Fig. 1). Considering that the MBETC are the only cells that contain both types of ingrowths and where the flange ingrowths are more extensive, the experiments focused on these cells.

Reticulate ingrowths

At 5 DAP and using TEM, in many sections, the cells of the placento-chalazal region were initiating reticulate ingrowth formations (Fig. 2a–b). However at the CLSM, most of the walls of the cells from this region labeled lightly and uniformly with calcofluor white (data not shown), unlike later development stages where the ingrowths were clearly identified (Fig. 2c, e, g). Reticulate ingrowths started developing at this stage, with the formation of randomly distributed initiation sites (Fig. 2a–b), but rapidly increasing their numbers to a point that they no longer could be individualized (6 DAP, Fig. 2c–d). The initiation sites were normally characterized by the formation of papillae (Fig. 2a), as described in previous studies (Talbot et al. 2007b; Vaughn et al. 2007), but sometimes they formed loop-like structures (Fig. 2b) that eventually fused with the adjacent ingrowths and created a fenestrated layer of less electron dense material than the adjacent OPW (Fig. 2d). The observations of the CLSM suggest the presence of short and mixed structures of cellulose material abound on the cytoplasmic side of the OPW at 6 DAP (Fig. 2c). Electron dense material from vesicles apparently flowed into the ingrowths starting at 6 DAP (Fig. 2d) and they probably originated from the Golgi apparatus.

At 7 DAP in most of the analyzed cells, the reticulate ingrowths had expanded approximately 5 μm into the cytosol (Fig. 2e–f). Cellulose predominated mostly near the

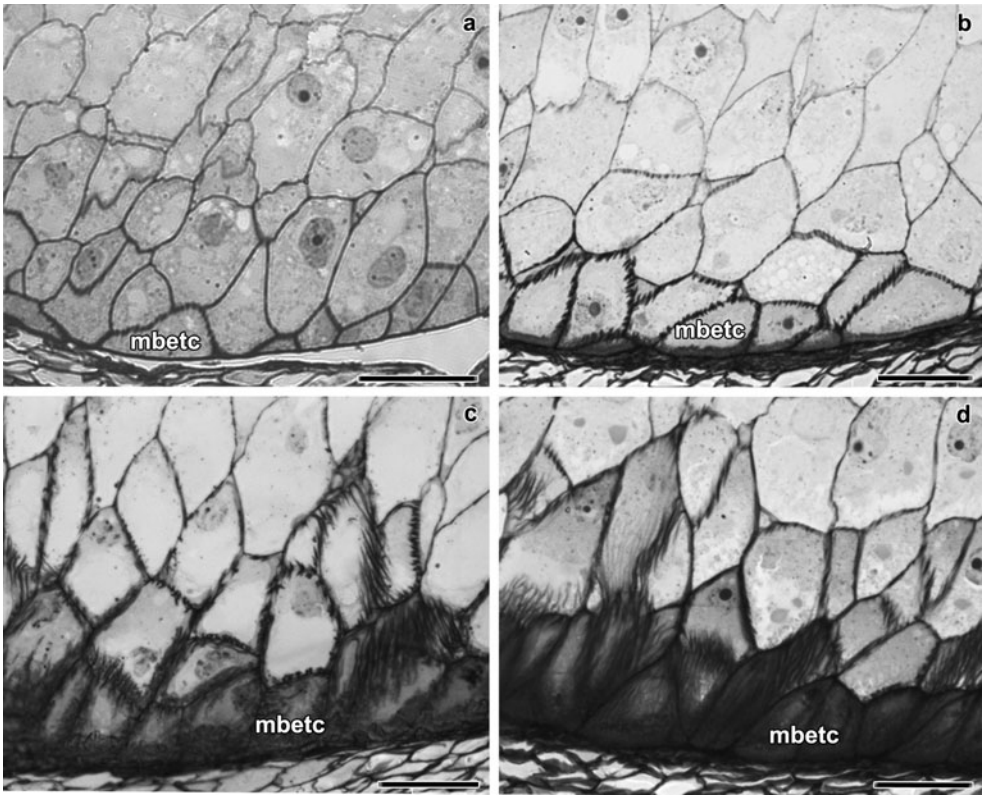

Fig. 1 Bright filed microscopy of longitudinal sections of maize endosperm transfer cells at 6 DAP (**a**), 10 DAP (**b**), 14 DAP (**c**), and 20 DAP (**d**). MBETC: most basal endosperm transfer cells. *Scale bars*=50 μm

OPW, whereas in the inner side multiple vesicles fused with the ingrowths (Fig. 2f). This is a period of active development of the ingrowths, where a complex labyrinth is still being formed next to the OPW and up to 5 μm of the adjacent anticlinal walls.

As the kernels reached about one fourth of their development, at 10 and 12 DAP, reticulate ingrowths were almost fully developed (Fig. 2g–i), because they were very similar to those at 20 DAP (Fig. 2j; Davis et al. 1990; Talbot et al. 2002; Kang et al. 2009). The orientation of the cellulose microfibrils was variable, but they were predominantly perpendicular to the cell long axis (Fig. 2i–j). The labyrinth of reticulate ingrowths had expanded approximately 7 μm into the cytosol (Fig. 2g) and the spaces were mostly filled with mitochondria (Fig. 2i–j). However, even at 20 DAP, vesicles were still being added to the reticulate ingrowths (Fig. 2j), which is a sign that these ingrowths were still being formed, despite the observation that their expansion into the cytosol had not changed significantly from 10 to 20 DAP.

Flange ingrowths

Flange ingrowths were also initiated at 5 DAP (Fig. 3a–c) and were mostly located next to the anticlinal walls (at least 5 μm apart from the OPW) and inner periclinal walls. The initiation sites were dispersed, but contrarily to the reticulate ingrowths, the flange ingrowths remained mostly individualized later in development. These ingrowths were made of an electron dense material resembling the adjacent primary walls, sometimes forming a continuous stretch of wall material (Fig. 3c), which apparently was mostly cellulose. At this stage, the flange ingrowths were not usually detected with CLSM (data not shown).

At 6 DAP as the flange ingrowths expanded, part of the anticlinal walls more than doubled in their width (Fig. 3d–f). Ingrowths were predominantly longitudinal, thus causing extensive wall enlargement, except near the plasmodesmata (Fig. 3e–f). The expansion of flange ingrowths in the MBETC was variable: in some cells the anticlinal walls started showing a predominantly longitudinal cellulose microfibril orientation (Fig. 3g), whereas in others, the ingrowths have expanded and thickened to the point of projecting into the cytosol (Fig. 3h–i).

At 7 DAP, the ingrowths enlarged significantly; they were mostly formed of cellulose material (Fig. 3j–k) and vesicles were added to the growing edges (Fig. 3j). The orientation of cellulose microfibrils was essentially longitudinal, either of ingrowths adjacent to the anticlinal (Fig. 3j–k) or inner periclinal walls (data no shown), which were mostly perpendicular to the microfibrils of the reticulate ingrowths (Fig. 2j–k). Frequently, newly added microfibrils ran parallel to the existing ones of the adjacent primary wall, but at some point they detached from them and projected inwards (Fig. 3k).

As the transfer cells progressed in their development, at 10 and 12 DAP, cellulose remained an important constituent

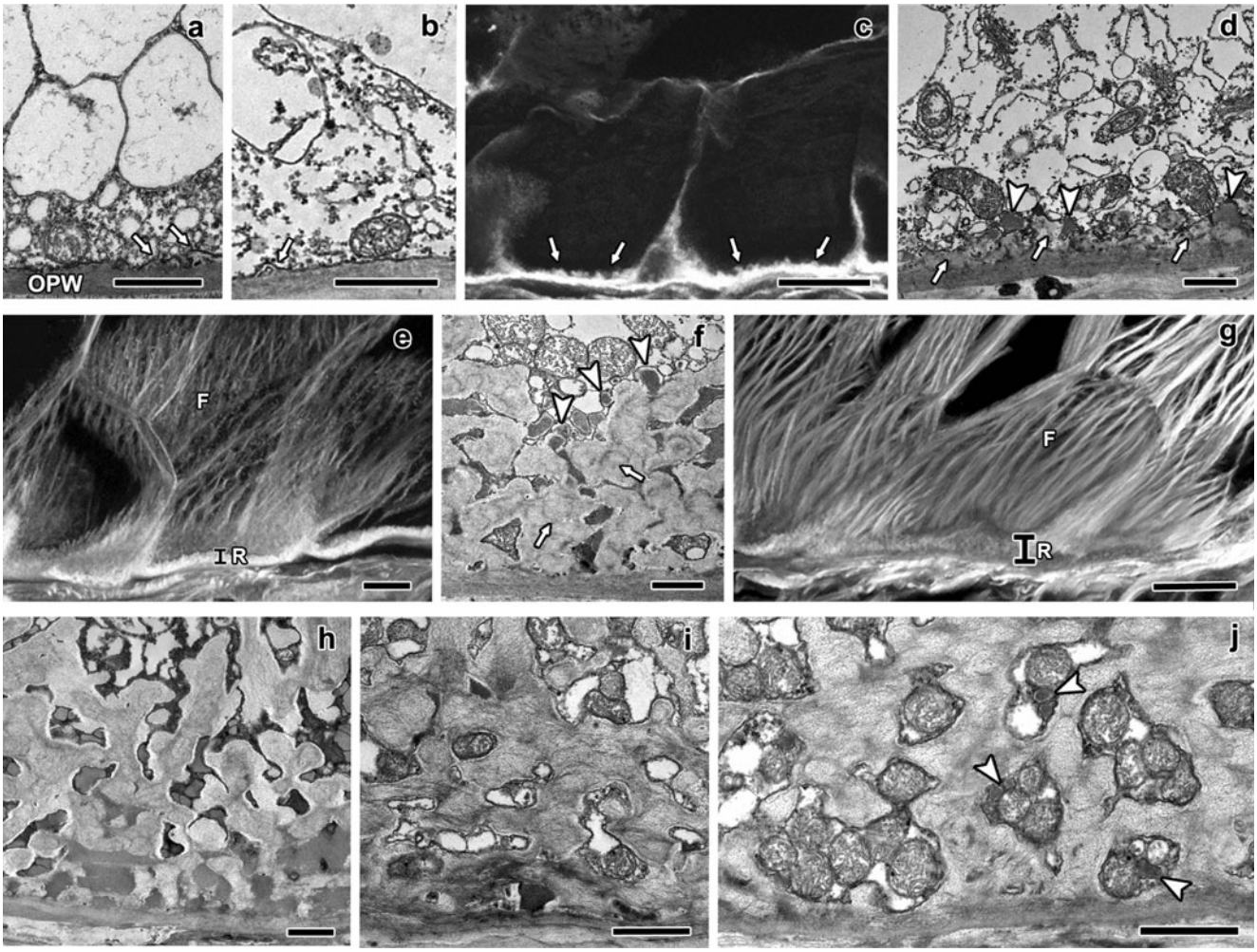

Fig. 2 Longitudinal sections of maize endosperm transfer cells' reticulate ingrowths from 5 to 20 DAP. The images **a**, **b**, **d, f**, **h–j** were obtained with TEM, whereas the images **c**, **e**, and **g** were obtained with CLSM. **a–b** sections of the MBETC at 5 DAP with newly formed papillae (**a**, *white arrows*) or loop-like structures (**b**, *white arrows*) adjacent to the OPW. **c** section of two of the MBETC at 6 DAP in which the reticulate ingrowths cover most of the cytoplasmic side of the OPW (*white arrows* pointing more generally the reticulate ingrowths, than in images **a** and **b**). **d** detailed sections of reticulate ingrowths (*white arrows*) forming at least one fenestrated layer with vesicles apparently fusing with it (*white arrow heads*) at 6 DAP. **e** section of transfer cells at 7 DAP in which there was a clear separation between the reticulate (*R*) and flange ingrowths (*F*). **f** detailed images of the labyrinth of reticulate ingrowths (*white arrows*) at 7 DAP, the spaces within were filled with material with electron density similar to the included in vesicles that were apparently still fusing with it (*white arrow heads*). **g** section of the MBETC at 10 DAP, still denoting a clear separation between the reticulate (*R*) and flange ingrowths (*F*). **h** detailed image of the labyrinth at 10 DAP with electron dense material filling most of the spaces within. **i** detailed image of the labyrinth at 12 DAP with mitochondria filling most of the spaces and cellulose microfibrils mostly oriented perpendicularly to the cell long axis, although they have different orientations and they are not very densely packed. **j** detailed image of the labyrinth at 20 DAP, mitochondria still fill the spaces in between, but there are also vesicles (*white arrow heads*) apparently being added to these structures and other cell components that cannot be identified. *OPW*: outer periclinal wall; *white arrow*: reticulate ingrowth; *white arrow head*: vesicles apparently being added to expanding ingrowths; *R*: reticulate ingrowths region; *F*: flange ingrowths. *Scale bars*: **a**, **b**, **d**, **f**, **h–j**=1 μm; **c**, **e**, **g**=20 μm

of the ingrowths, unlike the reticulate ingrowths the microfibrils were closely packed (Fig. 3l) and were essentially longitudinally oriented (Fig. 3m–n). The mostly longitudinal or oblique flange ingrowths often extended as much as the anticlinal walls (Figs. 2g and 3m–n), thus forming anastomosed rib-like structures, as reported in other studies (Talbot et al. 2002, 2007a). However, in some cells (less than 10 %), microfibril and ingrowth orientation was transverse to the long axis of the cell (Fig. 3n), but it is not clear how this occurred.

At mid-endosperm development (20 DAP), the MBETC did not appear changed from previous stages (10–12 DAP), except that the flange ingrowths have evolved from the more distal part of OPW to the region where the reticulate ingrowths exist, often overlapping them and filling much of the cytosol (Fig. 3o). The flange ingrowths' microfibrils were oriented

transverse to the cell long axis, but apparently that was due to bending of these structures, because as they approached the reticulate ingrowths, probably due to space constraints, they curved as did their microfibrils (Fig. 3o). The inner transfer cells continued having a much lower quantity of ingrowths than the MBETC (Fig. 1); the ingrowths were exclusively flange and became more extensive and interwoven as these cells developed (Figs. 1 and 3o). At this stage, plasmodesmata were mostly found in non-thickened regions of the primary wall, but occasionally were located in slightly thickened regions (Fig. 3p). It is not clear whether the plasmodesmata constrained ingrowth formation, or if they were restricted to regions of the primary wall that happened not to contain any ingrowths. Certainly, plasmodesmata exist between the most basal and inner transfer cells and they should contribute to assimilate flux to inner transfer cells.

Fig. 3 Longitudinal sections of maize endosperm transfer cells' flange ingrowths from 5 to 20 DAP. All images were obtained from the MBETC; images **g–i** and **m–o** also show inner transfer cells. The images **a–f**, **j–l,** and **o–p** were obtained with TEM, whereas the images **g–i** and **m–n** were obtained with CLSM. **a–c** detailed view of initiating flange ingrowths (*white arrows*) adjacent to the anticlinal walls (*AW*) at 5 DAP. **d–f** flange ingrowths at 6 DAP, but not developing near plasmodesmata (*black arrow heads*). **g–i** images of 6 DAP transfer cells with different stages of flange ingrowth (*white arrows*) development (**g** being in a less advanced stage of development and **i** in the most advanced stage of development with flange ingrowths clearly identified). **j–k** flange ingrowths (*white arrows*) at 7 DAP, the cellulose fibers are longitudinally oriented and run parallel to the adjacent anticlinal walls (*AW*, and usually parallel or oblique to the cell long axis), with vesicles added to their edges (*white arrow head*). **l** detail of 10 DAP flange ingrowths, where cellulose microfibrils were mostly longitudinally oriented, vesicles and mitochondria were abundant among them. **m–n** 10 DAP transfer cells with flange ingrowths mostly oriented parallel or oblique to the cell axis, although in some cases the flange ingrowths can be oriented transversely (*T*), as in image **n**. **o** general view of transfer cells at 20 DAP in which the flange ingrowths (*white arrows*) evolved to the reticulate ingrowths region (near the OPW), but there was still a clear separation between both types of ingrowths. **p** detailed view of the inner periclinal and adjacent anticlinal wall at 20 DAP where plamodesmata were visible in parts of the primary wall that were not thickened except two that were located in regions of the wall where thickening due to ingrowth formation occurred (*black arrows*). *AW*: anticlinal wall; *OPW*: outer periclinal wall; *white arrow*: flange ingrowth; *black arrow head*: plasmodesmus in regions of the anticlinal wall where there is no ingrowth development; *white arrow head*: vesicles apparently being added to expanding ingrowth; *T*: microfibrils transverse to the cell axis; *black arrow*: plasmodesmus in ingrowth expanded walls; *IPW*: inner periclinal wall. *Scale bars*: **a**, **e**, **j–l**, **p**=1 μm; **b**=250 nm; **c**, **f**= 500 nm; **d**, **o**=5 μm; **g–i**, **m–n**=20 μm

Discussion

Ingrowth initiation started at 5 DAP, whereas it usually is reported to start around 6 DAP (Charlton et al. 1995; Becraft 2001). The difference may arise from the fact that the plants used in this study were grown in warmer conditions than previous studies, therefore they accumulated between 75 and 81 GDD in 5 days, which is approximately the same for 6 day grown kernels at an average temperature of 23.5 °C. However, we cannot rule out the possibility of the use of different genotypes contributes to differences in transfer cell developmental rates.

The reticulate ingrowths started as discrete papillae emerging directly from the OPW, their numbers increased and rapidly formed a fenestrated layer of apparently disorganized cell wall structures with various electron densities, but mostly less than in the adjacent OPW. These data suggest that the compaction of cell wall material in the reticulate ingrowths is less pronounced than in the adjacent OPW. Other layers were formed on top of this cell wall material creating a labyrinth that covered the cytoplasmic side of the OPW. The orientation of cellulose fibers in the reticulate ingrowths was variable, but predominantly transverse to the long axis of the cell. Apart from cellulose, other components were added, normally including vesicles that most likely originated from the Golgi apparatus. Unlike the seed coat of *Vicia faba* L. (Wardini et al. 2007; McCurdy et al. 2008), we have not observed a uniform wall layer on the cytoplasmic side of the OPW prior to or during reticulate ingrowth initiation (Monjardino et al. 2007; Fig. 2a–b). The variations in electron density of the OPW (Fig. 2a–b, d) were probably due to previous fusions of nucellar and integument cell walls (Monjardino et al. 2007) and they were thicker and more electron dense than the unified wall layer reported by Wardini et al. (2007).

The flange ingrowths started as localized enlargements of the anticlinal and inner periclinal walls, the electron density of the structures within was very similar to the adjacent primary walls and remained for further developmental stages. These ingrowths were essentially made of cellulose and other constituents probably originating from vesicles of the Golgi apparatus. Unlike the reticulate ingrowths, the flange ingrowths remained discrete from adjacent structures throughout development. They, were also formed in the inner two to six cells, the cellulose fibers were more densely packed throughout development and oriented longitudinally to the long axis of the cell, the ingrowths often expanded as much as the length of the cell (in some cases they reached 60 μm in length) and formed long rib-like structures that often were anastomosed.

The coexistence of reticulate and flange ingrowths in the MBETC is unique in that they arose from distinct locations (the reticulate ingrowths were located exclusively near the OPW and the adjacent 5–10 μm of the anticlinal walls, whereas the flange ingrowths were located mostly next to the remaining walls of these cells) and they were both formed at the same time. At least 95 % of the cells of this region contained both types of ingrowths. However, in a

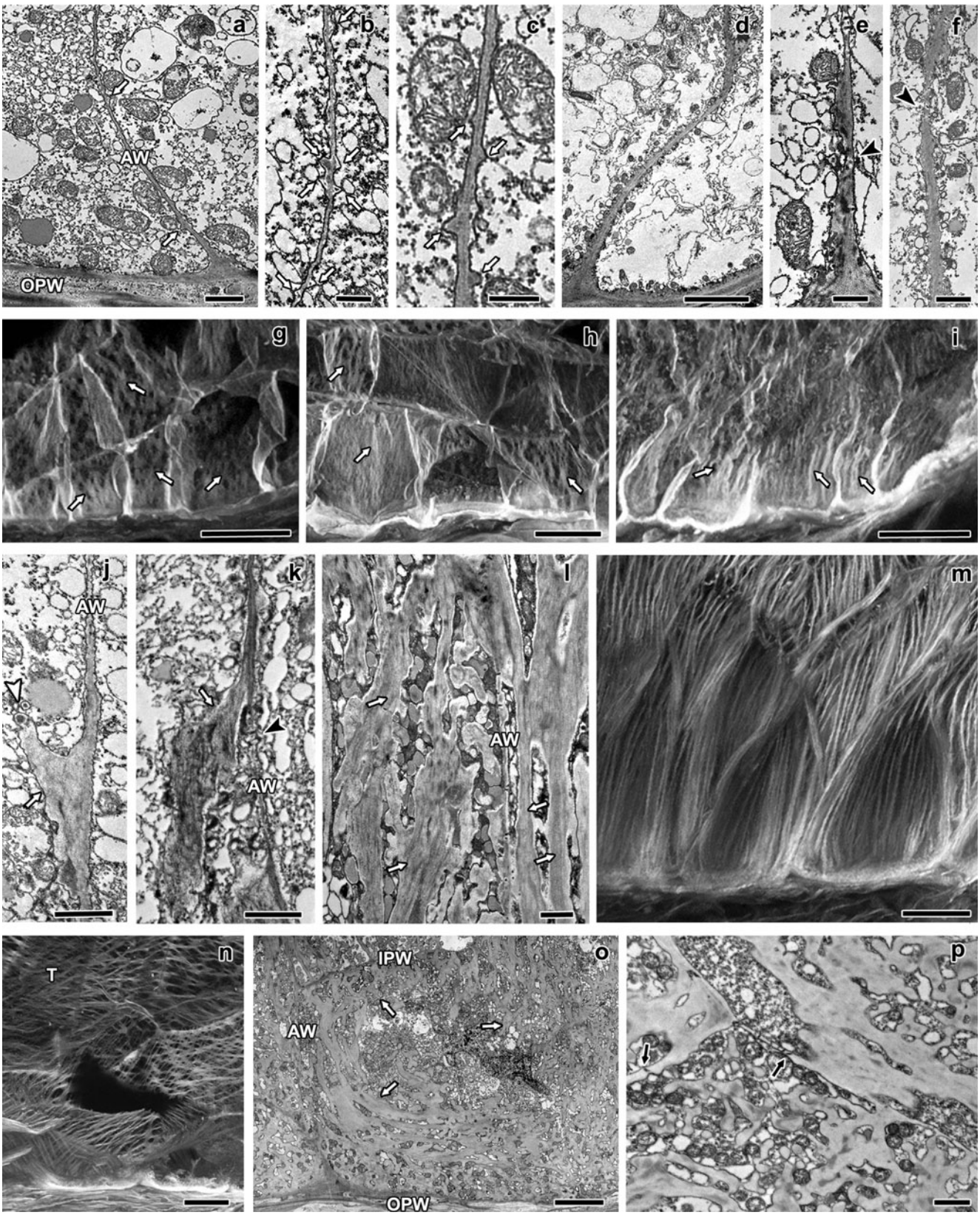

very limited number of samples (less than 1 %), we observed that both ingrowths arose from the OPW, but the presence of the reticulate ingrowths significantly outnumbered the flange ingrowths (data not shown). The

coexistence of both types of ingrowths in the same cells has been reported previously (Talbot et al. 2002; Pugh et al. 2010). In cells of nucellar projections of *Hordeum vulgare* L., the reticulate type is prevalent, but in some cells, both types coexist without clear separation between them (Talbot et al. 2002) as in maize endosperm transfer cells (Figs. 2 and 3). The transfer cells from the seed coat of *Gossypium hirsutum* L. also contain both types of ingrowths in the same cells, but the reticulate ingrowths are formed over the previously existing flange ingrowths (Pugh et al. 2010), which differs significantly from our data.

Felker and Shannon (1980), Griffith et al. (1987), Felker et al. (1990), and others have reported the prevalence of passive transport of sugars through these cells during maize kernel development, mostly due to the activity of cell wall-bound invertases (Thompson et al. 2001). It has been suggested by Cheng et al. (1996) that the sucrose gradient in MBETC must have a direct impact on the activity of the membrane-bound and soluble forms of invertase. Considering that the reticulate ingrowths are concentrated near the OPW, they may be more influenced by the concentration of sucrose or other assimilates than the flange ingrowths. Alternatively, the reticulate ingrowths may be more efficient than the flange ingrowths on assimilate uptake into the endosperm.

Sugars (mostly monosaccharides) are transported into the endosperm by diffusion and actively by membrane carriers (Felker and Goodwin 1988; Thompson et al. 2001). Mitochondria were still very abundant next to both ingrowths at 12 and 20 DAP (Figs. 2j–k and 3o–p), and their cisternae were intact (unlike the cellularization stages when the cisternae were barely visible; Monjardino et al. 2007), suggesting that they are active. In addition, to assist the synthesis of new cell wall material, which was still occurring at 20 DAP (Fig. 2k), these organelles must also have contributed to active transport of assimilates into the endosperm (Thompson et al. 2001). However, the extent by which it may occur is yet to be determined. Understanding more thoroughly the mechanisms of assimilate uptake into the endosperm may be greatly improved by considering the existence of the two types of ingrowths in maize endosperm transfer cells.

In conclusion, reticulate and flange ingrowths coexist from earlier stages of development in the MBETC; they always differ from each other at ultrastructural level and are located in different sites of the same cells. The inner transfer cells only develop flange ingrowths. The reticulate ingrowths form a fenestrated complex next to the OPW have less densely packed cellulose microfibrils with various orientations, but still predominantly transverse to the cell's long axis, and are developed at 12 DAP. The flange ingrowths develop for longer periods, at least until 20 DAP, the microfibrils are more densely packed, mostly oriented parallel or oblique to the cell long axis, and they form long and often interwoven structures. The coexistence of both types of ingrowths in maize MBETC, to our knowledge, has not been reported in any other species.

Acknowledgments This research was supported in part by the Instituto de Biotecnologia e Bioengenharia - Centro de Biotecnologia dos Açores, by Grant BIIC M3.1.6/F/038/2009 from Direcção Regional de Ciência e Tecnologia, and by Grant SFRH/BD/8122/2002 from Fundação para a Ciência e Tecnologia. The authors thank Richard M. Twyman and Alan G Smith for critical review of the article and to Fabíola S. Gil for her technical input.

Conflict of interest The authors declare that they have no conflict of interest.

References

Becraft PW (2001) Cell fate specification in the cereal endosperm. Cell Dev Biol 12:387–394. doi:10.1006/scdb.2001.0268

Becraft PW, Yi G (2011) Regulation of aleurone development in cereal grains. J Exp Bot 62:1669–1675. doi:10.1093/jxb/erq372

Charlton WL, Keen CL, Merriman C, Lynch AJ, Grennland AJ, Dickinson HG (1995) Endosperm development in *Zea mays*; implication of gametic imprinting and paternal excess in regulation of transfer layer development. Development 121:3089–3097

Cheng WH, Taliercio EW, Chourey PS (1996) The *Miniature*1 seed locus of maize encodes a cell wall invertase required for normal development of endosperm and maternal cells in the pedicel. Plant Cell 8:971–983. doi:10.1105/tpc.8.6.971

Dahiya P, Brewin NJ (2000) Immunogold localization of callose and other cell wall components in pea nodule transfer cells. Protoplasma 214:210–218. doi:10.1007/BF01279065

Davis RW, Smith JD, Cobb BG (1990) A light and electron microscope investigation of the transfer cell region of maize caryopses. Can J Bot 68:471–479. doi:10.1139/B90-063

DeWitt G, Richards J, Mohnen D, Jones AM (1999) Comparative compositional analysis of walls with two different morphologies: archetypical versus transfer-cell-like. Protoplasma 209:238–245. doi:10.1007/BF01453452

Felker FC, Goodwin JC (1988) Sugar uptake by maize endosperm suspension cultures. Plant Physiol 88:1235–1239

Felker FC, Shannon JC (1980) Movement of 14 C-labeled assimilates into kernels of *Zea mays* L. III. An anatomical examination and microautoradiographic study of assimilate transfer. Plant Physiol 65:864–870. doi:10.1104/pp.65.5.864

Felker FC, Liu K-C, Shannon JC (1990) Sugar uptake and starch biosynthesis by slices of developing maize endosperm. Plant Physiol 94:996–1001. doi:10.1104/pp.94.3.996

Gilmore EC, Rogers JS (1958) Heat units as a method of measuring maturity in corn. Agron J 50:611–615. doi:10.2134/agronj1958.00021962005000100014x

Griffith SM, Jones RJ, Brenner ML (1987) In vitro sugar transport in *Zea mays* L. kernels; I. Characteristics of sugar absorption and metabolism by developing maize endosperm. Plant Phys 84:467–471. doi:10.1104/pp.84.2.467

Gunning BES, Pate JS (1969) "Transfer cells" plant cells with wall ingrowths in relation to short distance transport of solutes—their occurrence, structure, and development. Protoplasma 68:107–133. doi:10.1007/BF01247900

Gunning BES, Pate JS (1974) Transfer cells. In: Robards AW (ed) Dynamic aspects of plant ultrastructure. McGraw-Hill, London, pp 441–479

Hoagland DR, Arnon DI (1938) The water-culture method for growing plants without soil. California Agricultural Experiment Station.

College of Agriculture. Circ. 347, University of California, Berkeley

Kang B-H, Xiong Y, Williams DS, Pozueta-Romero D, Chourey PS (2009) *Miniature1*-encoded cell wall invertase is essential for assembly and function of wall-in-growth in the maize endosperm transfer cell. Plant Phys 151:1366–1376. doi:10.1104/pp.109.142331

McCurdy DW, Patrick JW, Offler CE (2008) Wall ingrowth formation in transfer cells: novel examples of localized wall deposition in plant cells. Curr Opin Plant Biol 11:653–661. doi:10.1016/j.pbi.2008.08.005

Monjardino P, Machado J, Gil FS, Fernandes R, Salema R (2007) Structural and ultrastructural characterization of maize coenocyte and endosperm cellularization. Can J Bot 85:216–223. doi:10.11.39/B06-156

Offler CE, McCurdy DW, Patrick JW, Talbot MJ (2003) Transfer cells: cells specialized for a special purpose. Annu Rev Plant Biol 54:431.454. doi:10.1146/annurev.arplant.54.031902.134812

Pugh DA, Offler CE, Talbot MJ, Ruan Y-L (2010) Evidence for the role of transfer cells in the evolutionary increase in seed and fiber biomass yield in cotton. Mol Plant 3:1075–1086. doi:10.1093/mp/ssq054

Salema R, Brandão I (1973) The use of PIPES buffer in the fixation of plant cells for electron microscopy. J Submicrosc Cytol 5:79–96

Talbot MJ, Franceschi VR, McCurdy DW, Offler CE (2001) Wall ingrowth architecture in epidermal transfer cells of *Vicia faba* cotyledons. Protoplasma 215:191–203. doi:10.1007/BF01280314

Talbot MJ, Offler CE, McCurdy DW (2002) Transfer cell architecture: a contribution towards understanding localized wall deposition. Protoplasma 219:197–209. doi:10.1007/s007090200021

Talbot MJ, Wasteneys GO, McCurdy DW, Offler CE (2007a) Deposition patterns of cellulose microfibrils in flange wall ingrowths of transfer cells indicate clear parallels with those of secondary wall thickenings. Funct Plant Biol 34:307–313. doi:10.1071/FP06273

Talbot MJ, Wasteneys GO, Offler CE, McCurdy DW (2007b) Cellulose synthesis is required for deposition of reticulate wall ingrowths in transfer cells. Plant Cell Physiol 48:147–158. doi:10.1093/pcp/pcl046

Thompson RD, Hueros G, Becker H-A, Maitz M (2001) Development and function of seed transfer cells. Plant Sci 160:775–783. doi:10.1016/S0168-9452(01)00345-4

Vaughn KC, Talbot MJ, Offler CE, McCurdy DW (2007) Wall ingrowths in epidermal transfer cells of *Vicia faba* cotyledons are modified primary walls marked by localized accumulations of arabinogalactan proteins. Plant Cell Physiol 48:159–168. doi:10.1093/pcp/pcl047

Wardini T, Wang X-D, Offler CE, Patrick JW (2007) Induction of wall ingrowths of transfer cells occurs rapidly and depends upon gene expression in cotyledons of developing *Vicia faba* seeds. Protoplasma 231:15–23. doi:10.1007/s00709-007-0244-0

Young TE, Gallie DR (2000) Programmed cell death during endosperm development. Plant Mol Biol 44:283–301. doi:10.1023/A:1026588408152